*Journal of Industrial Aerodynamics*, 5 (1979) 159—177



# WIND LOADS ON A BUILDING MODEL IN A FAMILY OF SURFACE LAYERS*

T.C. CORKE and H.M. NAGIB

*Illinois Institute of Technology, Chicago, IL 60616 (U.S.A.)*

(Received August 9, 1978; accepted in revised form April 6, 1979)

## Summary

A family of simulated neutral atmospheric surface layers was used to determine the response, i.e., "sensitivity", of the wind loads on a building model, as well as the associated flowfield near it, to variations in the characteristics of these "test boundary layers". The detailed description of this family of surface layers and the general flowfield near the same building model have been presented in a companion paper [1]. In both papers results are presented for the building in two orientations with respect to the wind.

Mean and unsteady pressure profiles on all sides of the building model provided new insight into the complex mechanisms involved in the flowfield of such bluff bodies. Good accuracy of the unsteady pressure distributions and their spectral content was facilitated by a new technique for the removal of the ever-present sound contamination from low-level pressure signals, which was developed [2] in the course of this study. The pressure measurements, combined with the corresponding velocity surveys, reflected the primary features of importance that may be sensitive to the details of the mean or fluctuating characteristics of the surface layer. The results include: the variation in the size of the horse-shoe vortex at the base of the building; spectra of pressure fluctuations; and documented variations in the wake Strouhal frequency with changing boundary layer characteristics.

On the windward face of the building, the distribution of mean and fluctuating pressure coefficients is presented using different normalizations in an attempt to reach definitions which lead to universal results for a full range of simulated atmospheric conditions. The best of these utilizes weighted sums of the mean and turbulent streamwise velocity components of the approach surface layers.

## Introduction

A common practice utilized by architects and wind engineers in the prediction of wind velocities around, and loads on, a building or structure is the testing of a scaled model of the structure in a wind tunnel, while simulating the conditions occurring in the atmosphere at the proposed construction site. Such a simulation involves the modeling of the topographical features of the terrain near, and upstream of, the site. In addition, it generally aims at modeling selected long-time average gust characteristics and velocity profiles which represent the mean atmospheric conditions immediately upstream of

*Parts of this paper were presented at the Third U.S. National Conference On Wind Engineering Research, Gainesville, Florida, 1978.

the proposed location for various wind directions. Such a simulation, however, loses considerable information about changes in the flow around, and pressures on, the building due to excursions from the mean. As discussed in detail in the Introduction to the companion work by Corke et al. [1], it is these changes or the sensitivity to them in the building flowfield which ar of vital importance for proper wind tunnel simulations and which can lead to valuable design information.

A considerable amount of information has been gathered in regard to the mean and unsteady characteristics of the atmospheric boundary layer [3—7] Coupled with this, substantial momentum has gathered in the area of simula ing the atmospheric conditions in wind tunnels [8—11]. However, basic questions as to how well these simulations actually predict conditions occur in the atmosphere remain unanswered. In addition, because of the complexi of the atmospheric flowfield, e.g., the complicated structure of the atmosph ic surface layer resulting from boundary layers growing within boundary layers [11], many of the characteristics for which these simulations are aiming are either unknown or ambiguous due to contradictions in results fro atmospheric studies. One particular source of ambiguity involves the length scales of atmospheric turbulence [6]. However, such scales are of vital importance in measurements of fluctuating surface pressures on buildings [12,1 In light of these uncertainties, model testing should include the examination of the sensitivity of measured effects to changes in the characteristics of the simulated atmospheric surface layer. Such changing charabteristics should involve velocity profiles, turbulence levels, spectra and length scales in an attempt to "bracket" the variability of conditions occurring in the atmosphe This approach toward wind tunnel testing of structures subjected to high winds is termed "sensitivity testing".

Using this sensitivity testing approach, our objectives were to determine the mean and unsteady pressures on a simple building model immersed in a family of selected test layers, for which all of the above-mentioned characteristics have been documented [1]. The results were used in conjunction with the mean and turbulent velocity surveys of the companion paper [1] to identify and categorize the various flow modules of the flowfield and to establish their sensitivity to the documented changes in the test layer characteristics. Examples of these flow modules are the rolled up horseshoe-shaped vortex surrounding the base of the building, the delta-wing-type pair of vortic initiating from the two edges of the building roof near a corner facing the win the tornado-like vortices near the ground in the wake of the building, and the shear layers emanating from building sides as well as edges normal to the wind direction. We anticipated that the outcome of such a study would shed light on the types of mechanisms involved in the complex flows around bluff bodies in these complicated turbulent shear flows. In turn, such information might provide insight into controlling undesirable aspects of the building flow field. Finally, through a systematic approach, we aimed at obtaining a definition for the mean and unsteady pressure coefficients which would lead to the

of its good frequency response and compact size, allowing it to be mounted inside the Scanivalve cavity.

Both of the transducers were calibrated for static and dynamic pressure variations. In the case of the Setra transducer, the output was frequency compensated to obtain a flat frequency response out to a frequency of 230 Hz, beyond which the output drops at a rate of 40 dB/decade. The details of the calibration and frequency compensation are presented in Ref. 16.

In order to obtain high quality fluctuating pressure distributions, a new technique was utilized for the removal of any sound contamination from the low-level pressure signals. The technique utilizes a separate probe which is dynamically tuned to match the building-pressure system and which senses only the sound-related pressure component in the wind tunnel. The details of the technique are presented by Corke and Nagib [2].

## Wind loads on building model

Utilizing the same family of simulated surface layers employed in our companion paper [1], and the same coordinate system and wind-tunnel arrangement (see Fig. 8 of Corke et al. [1]), the results reported in the following sections were obtained. A complete set of data for all sides of the model in two wind orientations and four test boundary layers are included in a report by the same authors [16]. A comprehensive description of the four test layers is discussed in the same report and the companion paper [1]. Only selected cases of the pressure data are presented here to illustrate the phenomena involved. On all the figures, a small schematic representing the cross-section of the building model and the flow direction with respect to it, is provided. Also included is a shaded region denoting the face of the model, with respect to the flow direction, on which the pressures were measured.

### *Mean and fluctuating pressure distributions*

The vertical distribution of the mean pressure coefficient, $\bar{C}_p$, along the centerline of the windward face of the model for orientation I, is shown in Fig. 1. This figure displays the large changes in the positive pressures reflecting the variations between the mean velocity distributions of the four test boundary layers. The distribution of mean pressure coefficients along the vertical centerline of the upstream face of the model, for orientation II, is presented in Fig. 2. Again the sensitivity of these distributions to the test layer characteristics is exhibited. In particular, the stagnation point on the model is observed to move upwards as the test layer changes from "C—1" to "C—4". This trend is coincident with an increasing power-law exponent for the mean velocity profiles of the simulated surface layers and with increasing turbulence levels for those four test layers.

The horizontal distribution and vertical variation of the mean and fluctuating pressure coefficient on the leeward face of the building for orientation II are displayed in Fig. 3. This figure reveals that even the loads on the down-

collapse of the results of the mean and unsteady pressure measurements into unified distributions insensitive to the changing boundary layer characteristics.

## Experimental approach

The wind tunnel used in this study was the "IIT Environmental Wind Tunnel" which operates in the closed return mode thus permitting the utilization of two test sections. In particular, this investigation utilized the low-speed test section located near the downstream end of the return leg of the tunnel. The dimensions of this test section are 4 X 6 X 22 ft., and the free-stream velocity can be controlled at any speed up to 25 ft/s. For more details on the wind tunnel, the reader is referred to the report by Tan-atichat and Nagib [14]. As with our related work [1,14—16], the simulated atmospheric surface layers were generated with the aid of the counter-jet technique. Details on the counter-jet system and its application to wind engineering research are presented in the same references.

The building model was constructed from plexiglas to the same dimensions (7.75-in. high, 4-in. square) as the model used in the velocity surveys presented by Corke et al. [1] A total of 47 pressure taps were placed on two sides and the top face of the model. Their arrangement reflects our sensitivity testing approach in that the spacing between taps becomes progressively closer as they approach the edges and base of the model thus yielding good resolution of changes in the pressure distributions occurring across these regions of large gradients.

The model was mounted on the tunnel floor on a 3-ft.-diameter turntable which allowed 360° of rotation with an angular positioning accuracy of 3 min. of one degree. Two model orientations were used in this investigation. In orientation I, the model has the diagonal of its cross-section aligned with the mean flow and in orientation II, one of its sides is facing the flow. For each orientation, the primary faces of the pressure tapped model were placed at different face locations with respect to the wind to obtain a complete survey of the wind loads on the model.

To collect pressures from the 47 taps of the model and to channel them to a pressure transducer, a 48 port Scanivalve (Scano #48D3—1/BCD/53—48) pressure scanner was used. The valve was mounted inside the model in the tunnel test section and connected to the pressure taps by equal lengths of 8.26-in.-long, 0.063-in.-I.D. tubing.

To measure the mean component of pressure, a Validyne DP45 Pressure Transducer, sensitive to a maximum differential pressure of 1 inch of water, was used. Because of its size, this transducer did not fit into the Scanivalve cavity. Therefore an adapter mounted inside the cavity and an additional 1.5 inches of 0.63-in.-I.D. tubing were used to channel the pressure to the transducer mounted next to the valve. For measuring the fluctuating component of pressure a Setra Model 237 pressure transducer, sensitive to a maximum differential pressure of 0.1 psid., was used. This transducer was chosen because

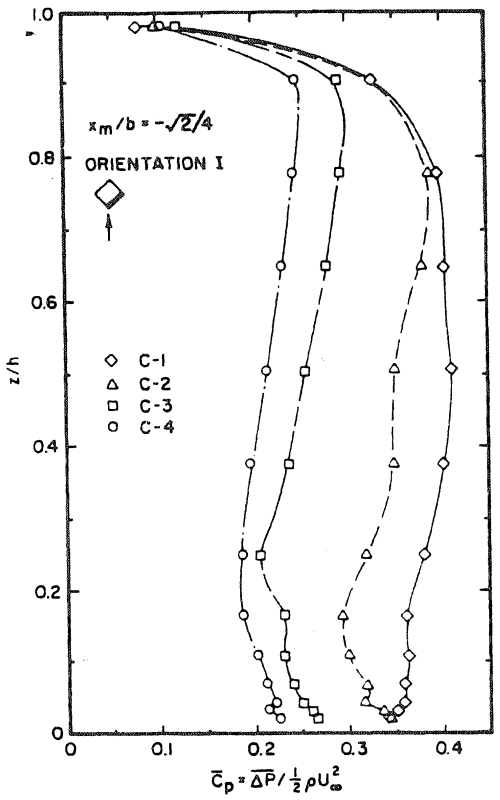


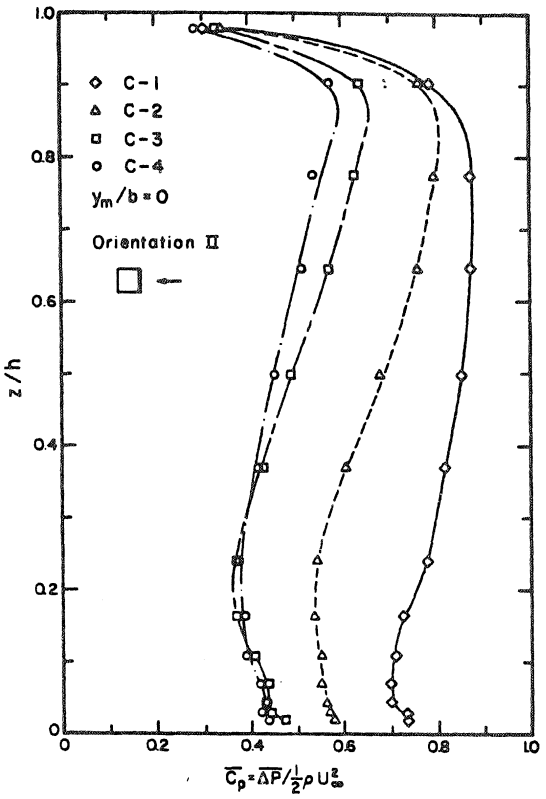


Fig. 1. Vertical distribution of mean pressure coefficient along centerline of windward face of building for orientation I.

Fig. 2. Vertical distribution of mean pressure coefficient along centerline of windward face of building for orientation II.

wind side of the building are highly dependent on the boundary layer characteristics. In particular, the sensitivity of the magnitude of the negative pressure distribution and its variation with height (closed symbols) is demonstrated.

A comparison of the magnitude of the pressure differences between the windward and leeward building faces in Figs. 2 and 3 indicates a net decrease in the drag on the building as the turbulence levels in the test layers increase. This result was also brought out by the velocity surveys in the wake of the building in our companion paper [1]. Similar observations have been made by Gartshore [17] and Laneville et al. [18]. They utilized turbulence generators upstream of a bluff body to demonstrate the more rapid reattachment of the shear layers in the case of the higher upstream turbulence level. Mean and unsteady pressure measurements on the side faces of the building [16] uphold this trend.

The vertical distribution of the "fluctuating pressure intensity" on the upstream face of the building for orientation II is shown in Fig. 4. This type of nondimensionalization of the fluctuating-pressure rms is analogous to the definition of turbulence intensity of velocity fluctuations. While the original data have been also presented [16] using the traditional method of $C'_p$ alone,

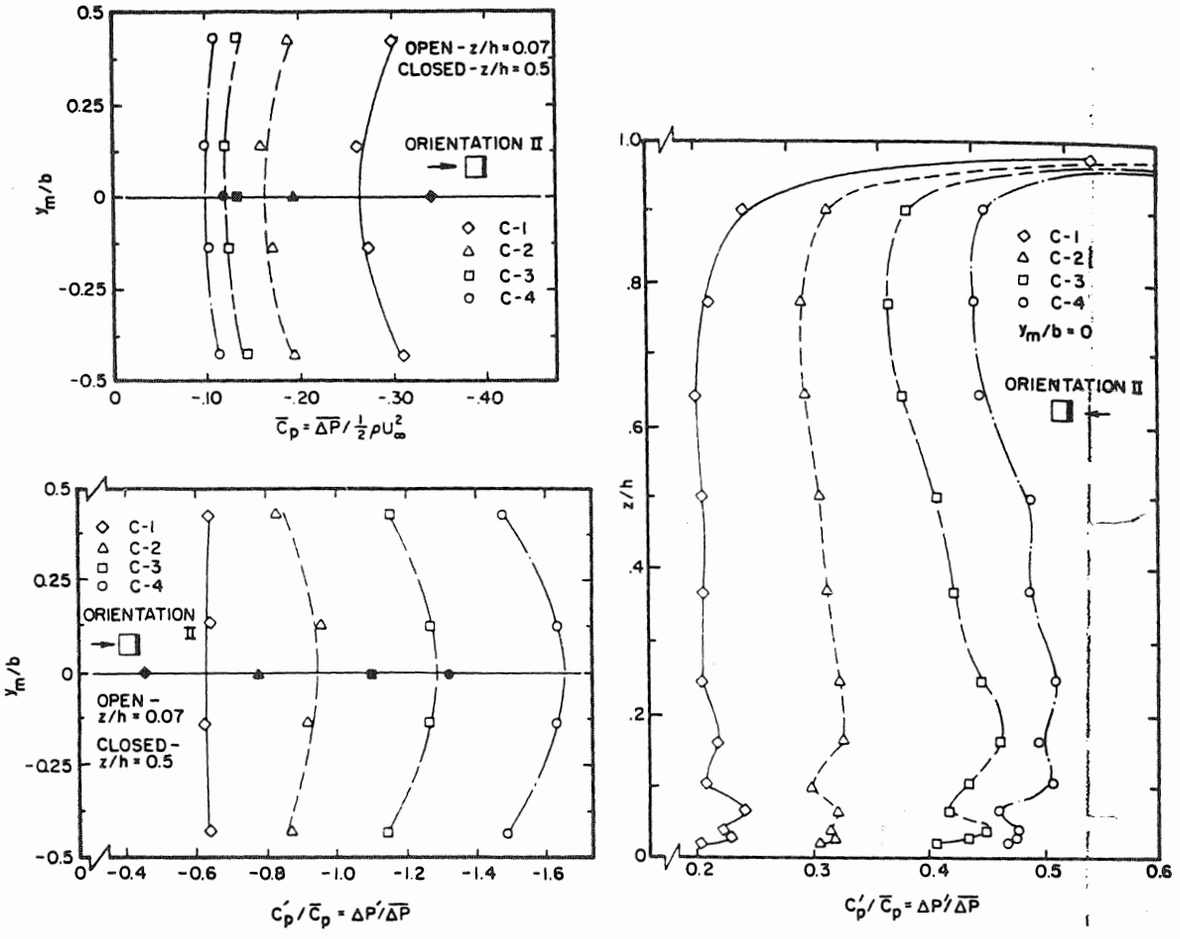


Fig. 3. Horizontal distribution and vertical variation of mean pressure coefficient and fluctuating pressure intensity on leeward face of building for orientation II.

Fig. 4. Vertical distribution of fluctuating pressure intensity along centerline of windward face of building for orientation II.

we have found the non-dimensionalization using $\overline{\Delta P}$ to be a more sensitive indicator of the differences in the flowfield as they are reflected in the unsteady pressure distribution on the building. In any case, a knowledge of any two of the pressure coefficients $\bar{C}_p$ and $C_p'$ and the fluctuating pressure intensity $C_p'/\bar{C}_p$ is adequate to establish all of them. Again, large magnitude variations, reflecting the differences in the unsteady velocities occurring in the test boundary layers, are revealed in Fig. 4. In addition, the peaks measured in the distributions near the base of the model indicate the presence of a rolled-up horse-shoe vortex module. This vortex is visualized along with the location of the stagnation streamline for test layer "C—2" in the photograph of Fig. 5, which shows a side view of the flow upstream and over the model. This and all other photographs shown here have been recorded during long time exposures of the streaklines generated by a new smoke visualization technique [17] based on the evaporation of oil from a fine wire. The wire is stretched across any plane of the flowfield on a portable probe, which can

be moved by the tunnel traversing mechanism. The observations, therefore, are made in either vertical or horizontal planes depending on the orientation of the smoke-wire probe.

It is important to realize that such flow modules as these vortices, occurring at the base of the building as well as those occurring on top of the building in the flow condition visualized in Fig. 8, and all the separated shear layers of the building are efficient mechanisms for transferring velocity fluctuations in the simulated surface layer into pressure fluctuations on the building. Thus such vortices and shear layers, as they are being jostled around by the turbulence, leave a strong "imprint" in the fluctuating pressure distribution on the model. In light of this interpretation, one may surmise that the distributions of Fig. 4 reveal that the size of the "roller" is increasing as we move from test layer "C—1" through "C- 4". Thus, this increase in size is coincident with an increase in the power-law exponent of the test boundary layers. This has been confirmed by visual records of the building flowfield in several of these simulated surface layers.

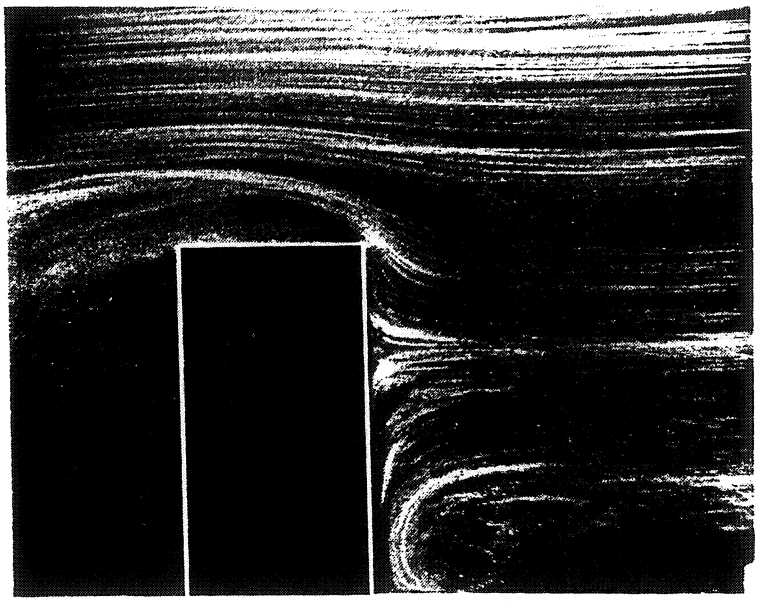


**Fig. 5. Visualization record showing flowfield in near upstream region of building in orientation II for test layer "C—2".**

Similar behavior has also been documented for the building in orientation I, as displayed in Fig. 6. The horse-shoe vortex flow module dominates the lower part of the flowfield around the building even when one corner of the model is facing the wind. This is a new finding of the present work which was somewhat surprising initially because of the weaker stagnation region of the building in this orientation. As depicted in Fig. 6, the size of the vortex grows

as the power-law exponent of the simulated surface layer is increased; a change which is concurrent with an increase in the turbulence level. The zone of influence of the vortex module extends as far as 40% of the height of the building in test layer "C—4".

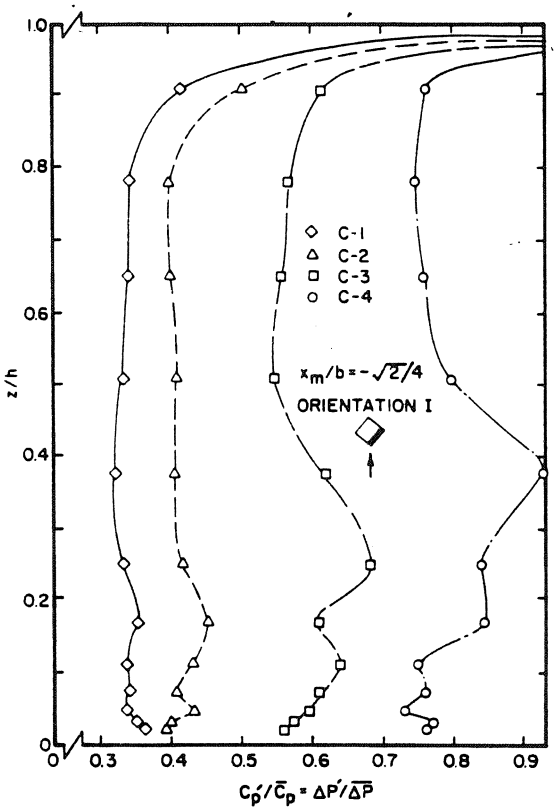


Fig. 6. Vertical distribution of fluctuating pressure intensity along centerline of windward face of building for orientation I.

Top views of smoke, introduced upstream of the model in a plane parallel to the ground at an elevation approximately 1/8 of the building height, confirm the existence of the horse-shoe vortex for both building orientations in Fig. 7. The general horse-shoe-like shape of the vortex is clearly visible in these photographs.

Moving the smoke-wire probe to an elevation just above the top of the building and locating it immediately downstream of the upstream corner of the model in orientation I, another of the flow modules is visualized. These delta-wing-type vortices develop along the upstream edges of the top and lead to substantial effects in the wind loads on the roof of the building. The distribution of the mean and fluctuating pressure coefficients, on top of the building along the diagonal aligned normal to the flow direction, are shown in Fig. 9. Here, the "imprint" of the rolled-up vortices coming over the top of the building is revealed. The strength of these vortices, which is reflected in both the mean and fluctuating pressure distributions, is highly dependent on the test layer characteristics. In particular, their intensity, as reflected by

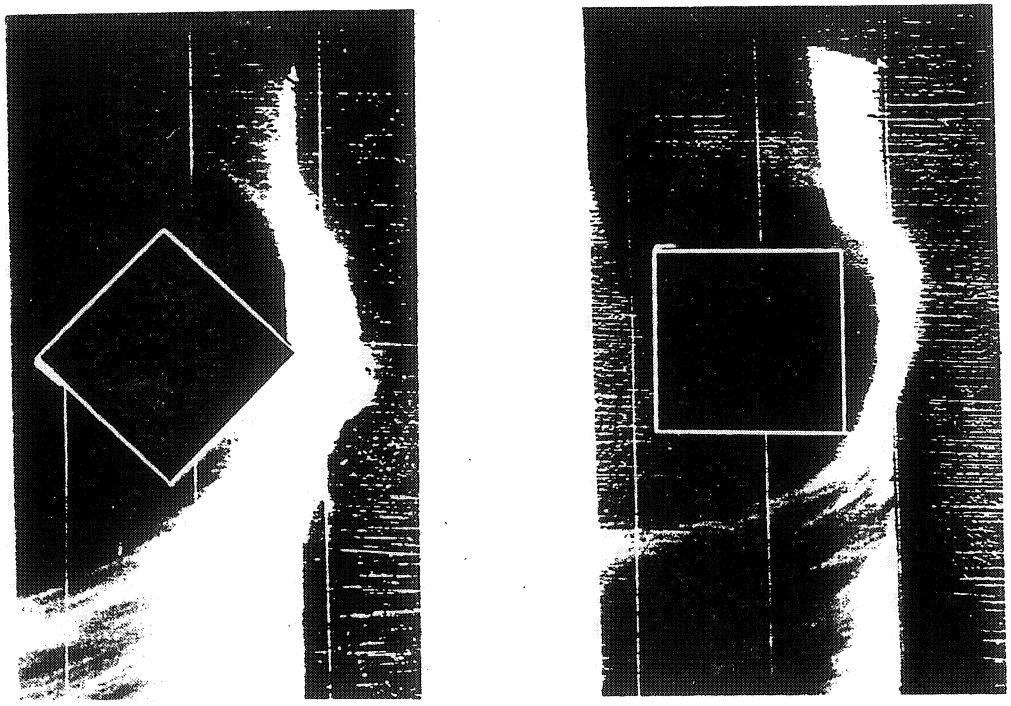


Fig. 7. Visualization records showing ground level flow field around building at two orientations in test layer "C—2".

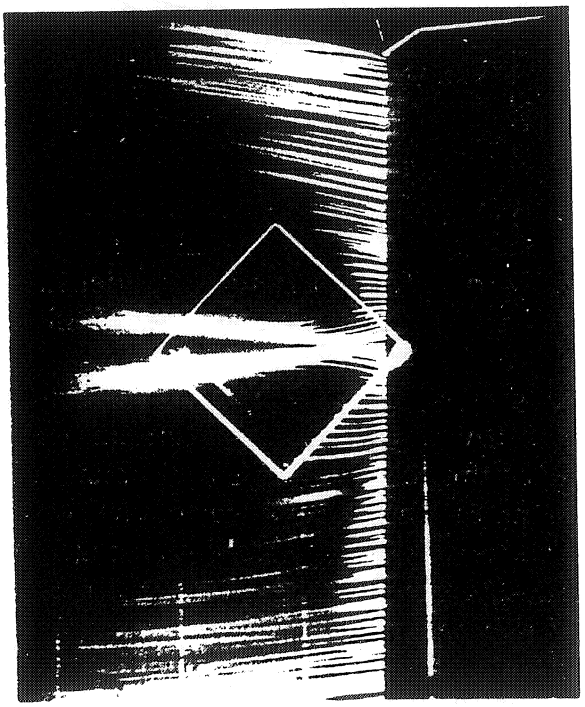


Fig. 8. Visualization record showing flowfield on top of building in orientation I for test layer "C—2".

the relative change in these coefficients across the span of the top of the model for each test layer, decreases with increasing turbulence levels. Velocity surveys have also indicated the same dependence on upstream conditions.

The sensitivity of the loads on the building to variations in the test layers has also been observed in the spectra of the fluctuating pressures. The spectra obtained from the pressure tap near the upstream corner at mid-height of the building in orientation I are presented in Fig. 10 for the entire family of surface layers. Here we observe an increase in the energy in the very low frequency range as the turbulence level of the test layer is increased from "C—1" to "C—4". This increase is balanced by a decrease in the energy in the intermediate range of frequency in these spectra, which have been normalized by the intensity of the pressure fluctuations in the corresponding test layer. Insignificant differences are recorded in the high frequency range, a finding which reflects the similar nature of the small-scale turbulence velocity fluctuations in the approach boundary layers [1].

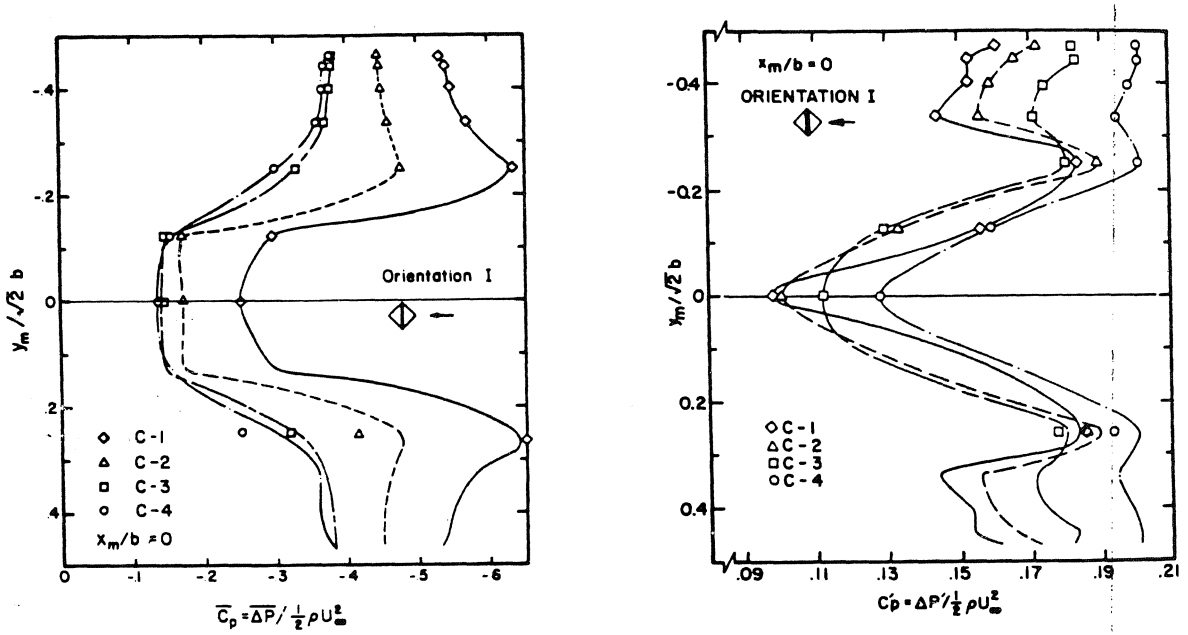


Fig. 9. Distribution of mean and fluctuating pressure coefficients on top of building along diagonal aligned normal to flow direction for orientation I.

In the spirit of the discussion on the velocity spectra in the companion paper [1], the selection of a suitable length necessary to non-dimensionalize the abscissa is left open to the reader. All parameters or length scales that may apply are available to the user of the results in this and the companion paper [1]. The corresponding scale in the prototype can then be used to complete the scaling.

Normalized spectra of pressure fluctuations occurring in the four test boundary layers on the upstream face of the building in orientation II are shown in the top part of Fig. 11 for a pressure port at the geometrical center

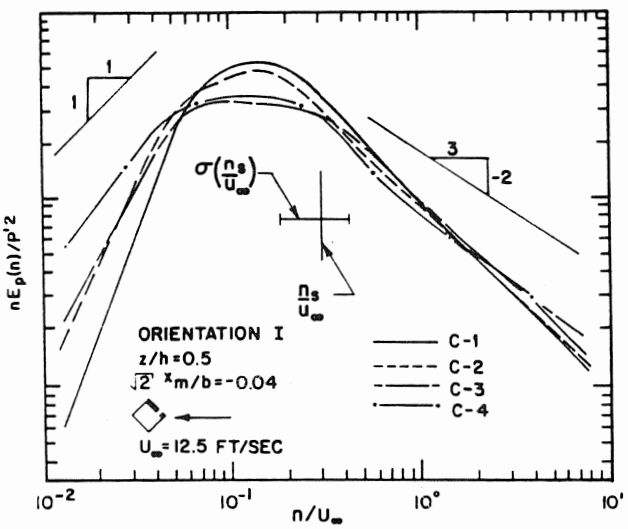


Fig. 10. Normalized spectra of pressure fluctuations near leading edge of windward face of building at half the building height and wake Strouhal frequency and its standard deviation for orientation I.

of the front of the model. These spectra also reveal small differences between the test boundary layers used in the higher frequency range. As for orientation I, significant variations in the spectra are measured at the lower frequencies. A comparison between the pressure spectra of Fig. 11 and the one-dimensional velocity spectra [1,16], taken upstream of the model also at approximately half the building height, indicates many similarities. For example, differences between the pressure spectra appear to be strongly tied to the low frequency variations occurring in the velocity spectra; i.e., tied to the energy-containing turbulence eddies in the test boundary layers. The bottom part of Fig. 11 displays the normalized spectra of pressure fluctuations sensed on the side face, at half the building height, for orientation II. Striking similarities in the general trends are observed between these and the comparable family of

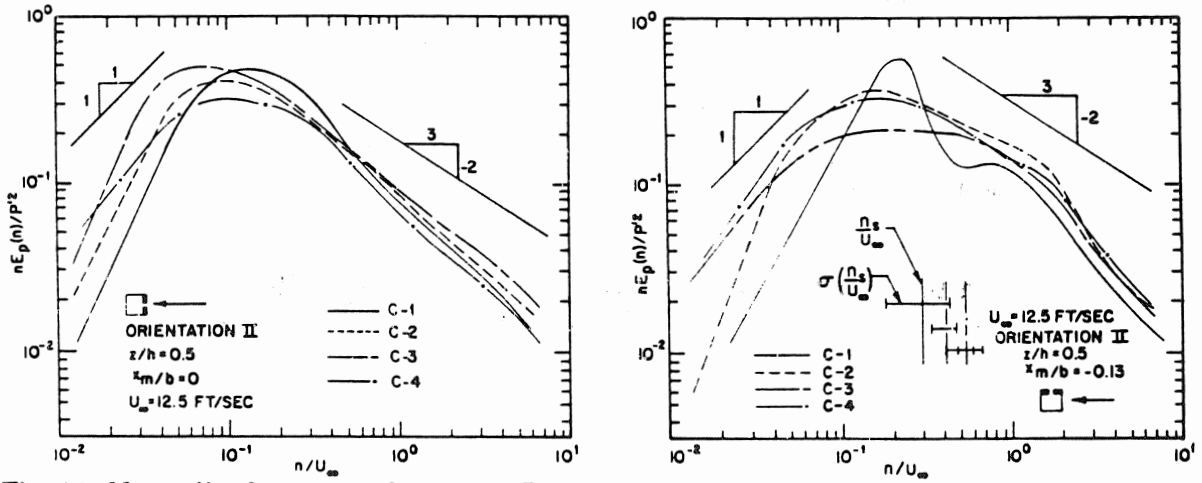


Fig. 11. Normalized spectra of pressure fluctuations on windward and side faces of building at half the building height, and wake Strouhal frequency and its standard deviation for orientation II.

f building-wake Strouhal number and its standard deviation with test layers and
on

| $\bar{S}_t = \bar{n}_s D/U_\infty$ | |
|---|---|
| Orientation | |
| I, $D = \sqrt{2}\, b$ | II, $D$ = b |
| 0.10 ± 0.04 | 0.10 ± 0.02 |
| — | 0.14 ± 0.03 |
| — | 0.18 ± 0.04 |
| — | 0.18 ± 0.02 |

Fig. 10, indicating the persistence of the same mechanisms discussed
her orientation of the building with respect to the wind. This leads
conclusion that the wind loads on the building depend strongly on
ter of the various flow modules in the building flowfield and their
n with the test layers.

cluded in Figs. 10 and 11 are the wake Strouhal frequency and its
deviation for all four test boundary layers as determined from the
induced pressure fluctuations on the side of the model. The shedding
was obtained by auto-correlating the output of a waveform eductor
riodically averaged the fluctuating pressure signal. The initiation of
ging cycle of the eductor was triggered by the eddy shedding-induced
he same pressure signal. The shedding in the wake of buildings of
ght in such highly turbulent flows is non-stationary in nature, being
d in amplitude and frequency (i.e., phase) and, therefore, would not
visible as a peak in the time-averaged spectral analysis of Figs. 10
The standard deviation of the Strouhal number is a result of this
on of the wake shedding frequency by the turbulence in the boundary
able 1 summarizes these results. The change of the Strouhal frequency
test layers represents the variation of the shear layers separating from
of the building, i.e., their diffusion and formation lengths, as a result
ing the turbulence level and scale in the simulated surface layer.

*of a universal pressure coefficient*

s indicated earlier in our list of objectives, we aimed at obtaining a
n for a pressure coefficient which would collapse the variations in
n and unsteady pressure distributions resulting from changing the test
aracteristics. The normalization of the pressure difference, $\overline{\Delta P}$, using
velocity $\bar{U}$ at the same height as the pressure port, which was
d in absence of the building model or sufficiently upstream of it, is
d as one such attempt in Fig. 12 for the windward face of the building
ation II. This definition collapses the profiles for three of the test
wn to approximately 50% of the building height. Below this value,

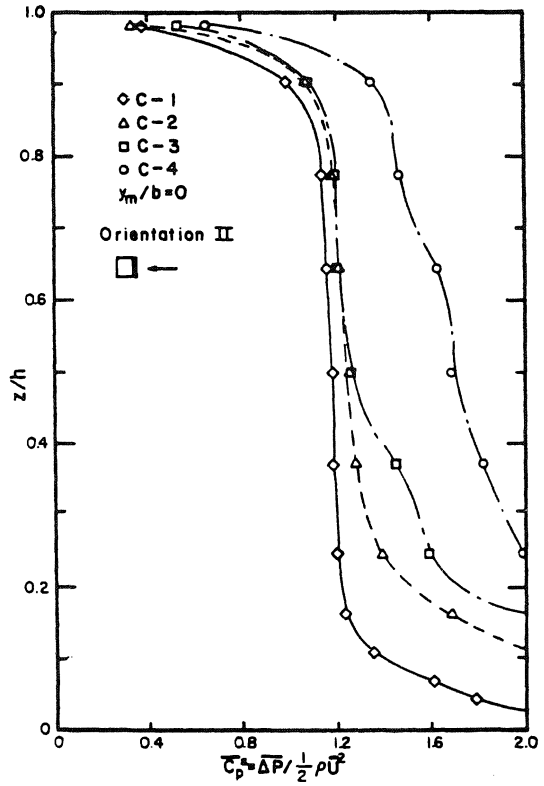


Fig. 12. Vertical distribution of local mean pressure coefficient on windward face of building in orientation II.

and over the entire building height for the fourth test layer, deviations indicative of wind loads not totally related to the on-coming *mean* velocity distribution are exhibited.

The problem with such a normalization is that it does not account for the differences in the turbulence levels between the test layers. We therefore chose a velocity pressure defined as $\frac{1}{2}\rho(\bar{U} + nu')^2$, where $\bar{U}$ and $u'$ are the mean velocity and the rms of the velocity fluctuations, respectively, taken sufficiently upstream of the building at the height of each of the pressure ports. The coefficient $n$ is a weighting factor used to account for the turbulence contributions to the wind loads. When $n$ equals zero we recover the definition presented in Fig. 12. We then adjust the value of $n$ to provide a best collapsing of the pressure distribution; i.e., a best unified distribution. As an indication of the degree of collapsing we define an error $\epsilon$:

$$\epsilon_{CC_p} = 1 - \frac{\min CC_p}{\max CC_p}$$

where $CC_p$ indicates a corrected pressure coefficient. We chose to determine $\epsilon$ for a port at half the building height which is representative of the collapse outside the region of the horse-shoe vortex at the base of the building. A tabulation of $\epsilon$ versus $n$ for mean and fluctuating pressure distributions on the windward face of the building for both orientations is presented in Table 2.

TABLE 2

Measure of scatter of pressure data at mid-height of building for different definitions of pressure coefficient

| $n$ | Orientation I | | Orientation II | |
|---|---|---|---|---|
| | $\epsilon_{CC_p}$ % | $\epsilon_{CC'_p}$ % | $\epsilon_{CC_p}$ % | $\epsilon_{CC'_p}$ % |
| 0 | 28.9 | 70.0 | 30.1 | 70.6 |
| 1 | 17.6* | 51.1 | 23.2* | 52.1 |
| 1.5 | 27.6 | 41.7 | 32.2 | 42.9 |
| 2 | 37.5 | 32.6 | 39.1 | 34.0 |
| 3 | 50.3 | 18.2 | 49.5 | 16.9 |
| 3.5 | 54.7 | 16.4 | 53.9 | 13.2 |
| 4 | 58.3 | 14.8* | 57.5 | 13.0* |
| 5 | 63.6 | 24.2 | 62.9 | 19.4 |
| 6 | 67.4 | 30.4 | 66.8 | 26.2 |
| 0, $U \rightarrow U_\infty$ | 47.9** | 19.1** | 47.0** | 20.8** |
| 0, $\bar{U} \rightarrow U_h$ | 20.1** | 56.1** | 26.2** | 57.1** |

*Best collapse.
**Much larger values of $\epsilon$ are found in the lower part of model.

As can be seen from Table 2, the best collapse occurs for $n = 1$ in the case of the mean pressures and $n = 4$ for the unsteady pressure distribution. These results are interesting in light of the commonly used practice of gust factors approximately equal to 3.5 and the recently suggested forms of an effective velocity for use in pedestrian comfort criteria [19]. Melbourne [20], in particular, recommends the use of $n = 3.5$, which is based on a 3-second wind speed reoccurrence along a Gaussian distribution of gust variations. These seemingly different approaches are essentially the same. All of them attempt to incorporate the turbulence energy into the measure of the wind loads on a structure or a person.

Using the best values for $n$, the distributions of the mean and fluctuating coefficients for the windward face of the building in orientation II are shown in Fig. 13 and 14. The mean coefficient for the windward face for the other orientation is presented in Fig. 15. The "good" degree of collapse of the data over the entire height of the building is gratifying.

Comparing Figs. 13 and 15, it is evident that a better collapse occurs in the case of orientation I. This trend was also evident from Table 2 and it can be explained by considering the modification of the flowfield due to the presence of the building. The mean and unsteady pressures on the building result from the mean and turbulent velocities in the boundary layer which are modified to some extent by the presence of the building. The magnitude of those modifications, which can be thought of as the sensitivity of the boundary layer to the building, is dependent on the boundary layer characteristics [1]. For example, Hunt [12] shows that the amplification of the turbulent velocity fluctuations depends on the building shape (or orientation) and on the scale

of the turbulence relative to the structure. The effective velocity, $\bar{U} + u'$, used in the normalization of $\overline{\Delta P}$ utilizes local quantities far upstream of the building. The modification of these, in particular $u'$, is minimal for the building in orientation I. Thus, we would expect a better collapse in the distributions for this orientation. The fact that this was confirmed by the data lends some credence to our use of this effective velocity.

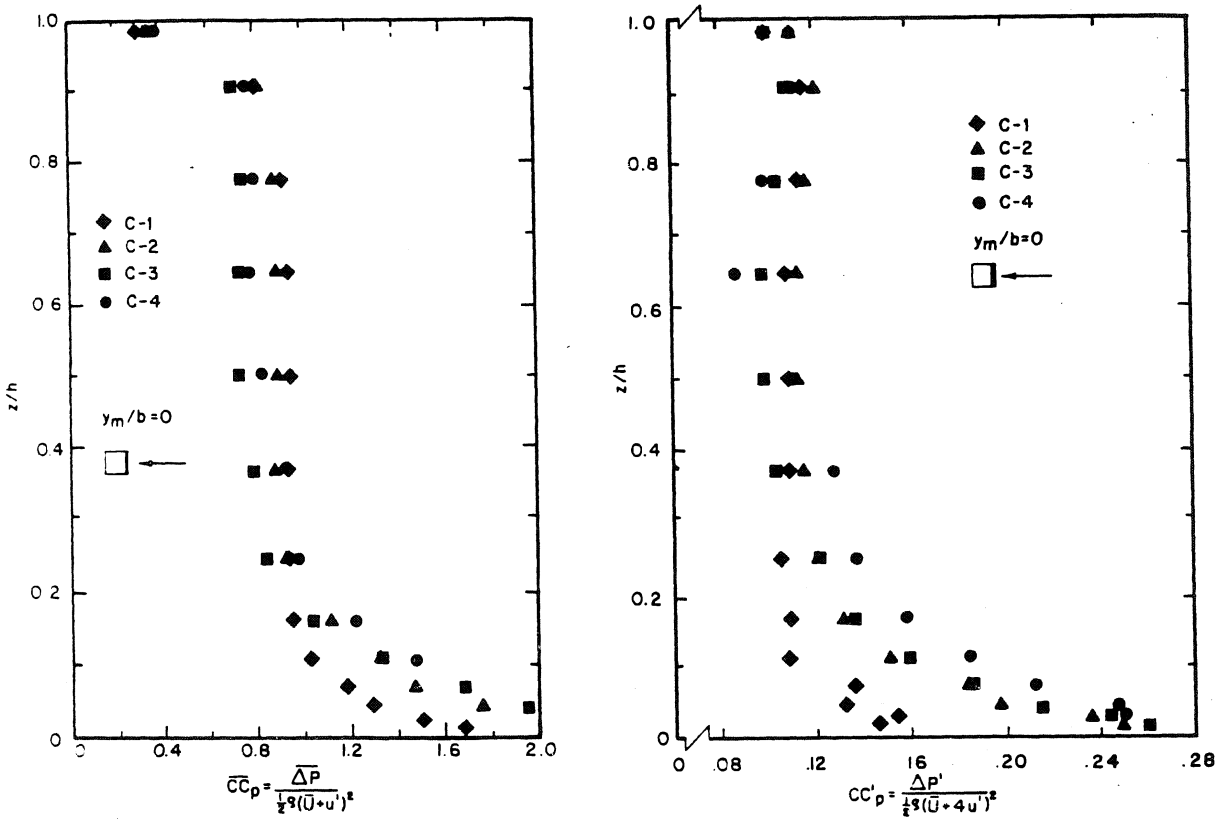


Fig. 13. Vertical distribution of corrected mean pressure coefficient ($n$=1) on windward face of building in orientation II.

Fig. 14. Vertical distribution of corrected fluctuating pressure coefficient ($n$=4) on windward face of building in orientation II.

A degree of collapse of the data from all four test layers similar to that shown here exists over the entire windward face of both building orientations. Utilizing the values of $n$, established for the best correlation of the mean and unsteady pressures along the windward side, we tested the corresponding pressure distributions over all faces of the building. From Figs. 13–15 one may select an acceptable maximum value of $\epsilon = 25\%$ as a criterion for a "good" correlation of the data. In orientation I the established values of $n$ result in "good" correlation over the entire model. The only exception is the mean pressure distribution on the roof of the building where $n = 0$ (instead of $n = 1$) leads to a better collapse. This particular value of $n$ suggests that the primary factor controlling the formation of the delta-wing vortices flow module is the mean velocity distribution, rather than the turbulence characteristics in the surface layer, which is a most significant result.

On the other hand, when the $n$ value from the windward face is used in orientation II, the mean pressure distributions only exhibit "good" collapse immediately downstream of separation lines, e.g., near the leading edges of the sides and roof of the building. All other surfaces of the model feature sensitivity which cannot be removed by this value of $n$. However, this does not limit this approach excessively since such zones near separation lines often feature the maximum suction on the building surfaces. Therefore, this method can still be utilized by designers to establish expected maximum wind loads for a range of atmospheric conditions based on a wind tunnel test in a single simulated surface layer. A better collapse of the corrected mean pressure coefficients on all sides of the building, other than the windward face, is achieved using $n = 0$.

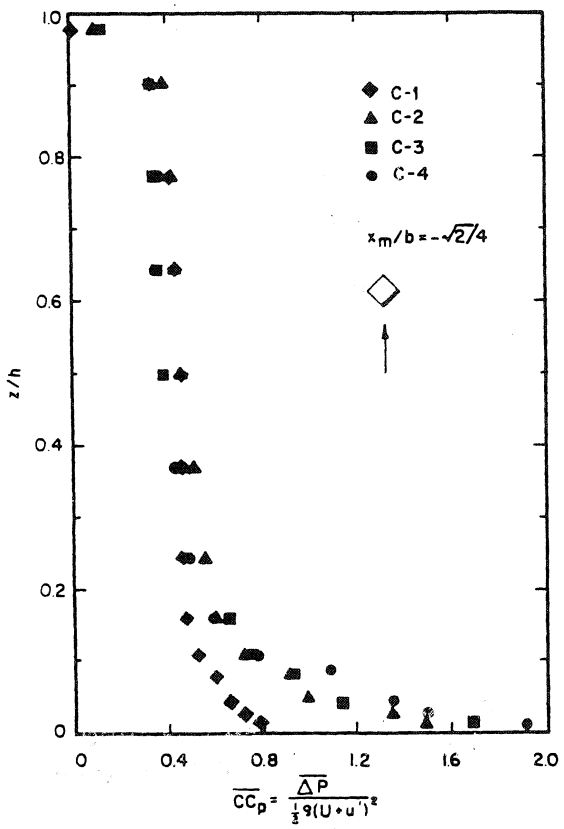


Fig. 15. Vertical distribution of corrected mean pressure coefficient ($n$=1) on windward face of building in orientation I.

"Good" correlation of all fluctuating pressure distributions in orientation II has been achieved using $n$ values determined from the windward face of the model, e.g., $n = 3$, see Table 2.

In closing it should be pointed out that using the corrected pressure coefficients proposed here always leads to improved correlation of all of the data collected in this investigation. It would be interesting to see if other data, e.g., Castro and Robins [22] and Akins [23], can be collapsed in a similar fashion and possibly correlated with the present data using this approach.

Their data were obtained for similar but different building models using other wind tunnels and boundary layer simulation conditions.

## Concluding remarks

A family of simulated atmospheric surface layers, covering a wide range of mean profile exponents, was used to examine the response of the flowfield around a simple building model to variations in the characteristics of the turbulent layers. Salient features in the mean and unsteady pressures on its surface are documented for the different boundary layers to establish the sensitivity of the flowfield to typical atmospheric variability. The results suggest that critical structures should be designed for wind loads bracketing the extreme values obtained from a sensitivity study which accounts for the variability of atmospheric conditions at the proposed site. They also suggest that the definition of the pressure coefficients in building codes should incorporate the contributions of the turbulence in the atmospheric surface layer, possibly through an effective velocity which accounts for the mean and turbulence characteristics of the wind. Corrected mean and unsteady pressure coefficients that utilize such a velocity are proposed. Good collapse of the data from all simulated surface layers is achieved by these coefficients on all surfaces of the building model, in particular, in its orientation with respect to the wind leading to least distortion of the flow.

## Acknowledgments

We are very grateful to Mrs. Valerie Mattioli for her expert typing of the many drafts of this manuscript. The research reported here was supported by NSF Grant ENG 76—04112.

## Notation

| | |
|---|---|
| $b$ | width of square cross-section of building model = 4.0 inches |
| C—1, C—2, C—3, C—4 | four test boundary layers with different characteristics, see Ref. 1 |
| $\bar{C}_p$ | mean coefficient of pressure = $\overline{\Delta P}/\frac{1}{2}\rho U_\infty^2$ |
| $\bar{C}_p{}^*$ | local mean coefficient of pressure = $\overline{\Delta P}/\frac{1}{2}\rho U^2$ |
| $C'_p$ | rms coefficient of pressure = $\Delta P'/\frac{1}{2}\rho U_\infty^2$ |
| $CC_p$ | mean corrected coefficient of pressure = $\overline{\Delta P}/\frac{1}{2}\rho(\bar{U}+nu')^2$; where $n$ is a turbulence weighting factor |
| $CC'_p$ | rms corrected coefficient of pressure = $\Delta P'/\frac{1}{2}\rho(\bar{U}+nu')^2$; where $n$ is a turbulence weighting factor |
| $E_p$ | spectrum function of building pressure fluctuations |
| $h$ | height of building model = 7.75 inches |
| $n$ | frequency in cycles per second |
| $n_s$ | shedding frequency in building wake |

| | |
|---|---|
| $P$ | mean pressure component on building model |
| $p$ | fluctuating part of pressure component on building model |
| $p'$ | rms value of $p$ |
| $P_s$ | static pressure measured in tunnel free stream |
| $\overline{\Delta P}$ | mean pressure difference ($\overline{P-P_s}$) |
| $\Delta P'$ | rms value of pressure difference ($P-P_s$) |
| $S_t$ | Strouhal number = $n_s D/U_\infty$, where $D = b$ for orientation I and $\sqrt{2}b$ for orientation II |
| $U$, $V$, and $W$ | mean velocity components in cartesian coordinate system $x$, $y$ and $z$ respectively |
| $u$, $v$, and $w$ | fluctuating parts of velocity components in cartesian coordinate system $x$, $y$ and $z$, respectively |
| $u'$, $v'$, and $w'$ | rms values of $u$, $v$ and $w$ |
| $U_\infty$ | mean velocity of free stream of wind tunnel |
| $x$, $y$, and $z$ | cartesian coordinate system as measured from counter-jet manifold, from side-wall of wind tunnel and from floor of test section respectively; see Fig. 8 of Ref. 1 |
| $x_m$ | streamwise distance from vertical centerline of building model; see Fig. 8 of Ref. 1 |
| $y_m$ | transverse distance from vertical centerline of building model; see Fig. 8 of Ref. 1 |
| $\epsilon$ | error measure of corrected pressure coefficient 1 – (min $CC_p$/ max $CC_p$) |
| $\rho$ | density of air computed from ideal gas relation |

## References


1 T.C. Corke, J. Tan-atichat and H.M. Nagib. Flow near a building model in a family of surface layers, J. Ind. Aerodyn., 5 (1979) 139.

2 T.C. Corke and H.M. Nagib, A large signal-to-noise technique for unsteady pressure measurements, AIAA J. 17 (1) (1978) 86.

3 H.A. Panofsky, The atmospheric boundary layer below 150 meters, Annu. Rev. Fluid Mech., 6 (1974) 147.

4 J.L. Lumley and H.A. Panofsky, The Structure of Atmospheric Turbulence, Wiley, New York, 1964.

5 E.J. Plate, Aerodynamic characteristics of atmospheric boundary layers, U.S. Atomic Energy Commission Technical Information Center, Oak Ridge, Tennessee, 1972.

6 H.W. Teunissen, Characteristics of the mean wind and turbulence in the planetary boundary layer, University of Toronto, Institute of Aerospace Studies, UTIAS Review No. 32, 1970.

7 J. Counihan, Adiabatic atmospheric boundary layers: A review and analysis of data from the period 1880—1972, Atmos. Environ., 1 (9) (1975) 871—905.

8 J.E. Cermak, Applications of fluid mechanics to wind engineering — A Freeman Scholar Lecture, J. Fluids Eng., 97 (1) (1975) 9—38.

9 A.G. Davenport and N. Isyumov, The application of the boundary layer wind tunnel to the prediction of wind loading, Paper No. 7, Wind Effects of Buildings and Structures, Proc. Int. Research Seminar at N.R.C. Canada, Univ. of Toronto Press, 1967.

10 J.C.R. Hunt and H. Fernholz, Wind-tunnel simulation of the atmospheric boundary layer: A report on Euromeck 50, J. Fluid Mech., 70 (1975) 543—599.

11 H.M. Nagib, M.V. Morkovin, J.T. Yung and J. Tan-atichat, On modeling of atmospheric surface layers by the counter-jet technique, AIAA J., 14 (2) (1976) 185.
12 J.C.R. Hunt, Turbulent velocities near and fluctuating surface pressures on structures in turbulent winds, Fourth International Conference on Wind Effects on Buildings and Structures, Cambridge University Press, 1977, p. 309.
13 J.O. Hinze, Turbulence, An Introduction to Its Mechanism and Theory, McGraw-Hill, New York, 1959.
14 J. Tan-atichat and H.M. Nagib, Measurements near bluff bodies in turbulent boundary layers intended to simulate atmospheric surface layers, I.I.T. Fluids and Heat Transfer Report R72—2, AFOSR—TR—74, 1974, (NTIS Publication AD782090).
15 J. Tan-atichat and H.M. Nagib, Wind tunnel simulation of neutral atmospheric surface layers by the counter-jet technique, J. APCA, 26 (7) (1976) 668.
16 T.C. Corke and H.M. Nagib, Sensitivity of flow around and pressures on a building model to changes in simulated atmospheric surface layer characteristics, I.I.T. Fluids and Heat Transfer Report R76—1, 1976, (NTIS Publication PB 267909/AS).
17 T. Corke, D. Koga, R. Drubka and H. Nagib, A new technique for introducing controlled sheets of smoke streaklines in wind tunnels, Proc. Int. Congress on Instrumentation in Aerospace Simulation Facilities, IEEE Publication 77 CH1251—8 AES, 1977, p. 74.
18 I.S. Gartshore, The effects of free stream turbulence on the drag of rectangular two-dimensional prisms, Research Report, Boundary Layer Research Laboratory, The University of Western Ontario, London, Canada, 1973.
19 A. Laneville, I.S. Gartshore and G.V. Parkinson, An explanation of some effects of turbulence on bluff bodies, Fourth International Conference on Wind Effects on Buildings and Structures, Cambridge University Press, 1977, p. 333.
20 T.V. Lawson, Session 5 Discussion—Environmental Effects, Fourth International Conference on Wind Effects on Buildings and Structures, Cambridge University Press, 1977, p. 478.
21 W.H. Melbourne, Criteria for environmental wind conditions, J. Ind. Aerodyn., 3 (1978) 241.
22 I.P. Castro and A.G. Robins, The flow around a surface-mounted cube in uniform and turbulent streams, J. Fluid Mech., 79 (1977) 307.
23 R.F. Akins, Wind pressures in buildings, Ph.D. Dissertation, Fluid Mechanics and Wind Engineering Program, Colorado State University, 1976.